

Relativistic Expansion of Electron-Positron-Photon Plasma Droplets and Photon Emission

R. Yaresko^{1,2,*}, Munshi G. Mustafa^{1,3,†} and B. Kämpfer^{1,2‡}

¹*Forschungszentrum Dresden-Rossendorf, 01314 Dresden, Germany*

²*Institut für Theoretische Physik, TU Dresden, 01062 Dresden, Germany*

³*Theory Division, Saha Institute of Nuclear Physics,*

1/AF Bidhannagar, Kolkata 700064, India

Abstract

The expansion dynamics of hot electron-positron-photon plasma droplets is dealt with within relativistic hydrodynamics. Such droplets, envisaged to be created in future experiments by irradiating thin foils with counter-propagating ultra-intense laser beams, are sources of flashes of gamma radiation. Warm electron-positron plasma droplets may be identified and characterized by a broadened 511 keV line.

PACS numbers: 12.20.-m, 52.50.Jm, 52.27.Ny, 52.25.Os

Keywords: Quantum Electrodynamics, Laser, Relativistic plasma, Gamma radiation and absorption

*Electronic address: r.yaresko@fzd.de

†Electronic address: musnigolam.mustafa@saha.ac.in

‡Electronic address: kaempfer@fzd.de

I. INTRODUCTION

The rapid progress in ultra-intense laser technology [1] triggered the interest in properties of relativistic plasmas consisting mainly of electrons (e^-), positrons e^+ and photons (γ). For instance, in [2–5] various processes, including thermal (kinetic) and chemical equilibration, have been considered for a hot charge-symmetric electron-positron-photon ($e^-e^+\gamma$) plasma, while the kinetics of a temporarily created electron-positron plasma has been analyzed in [6]. Hot plasmas, may be charge-symmetric or asymmetric or with ion load, have interesting features [7], e.g. with respect to collective excitation modes (including the van Hove singularity), astrophysical situations and secondary particle (such as muon or pion) production. Furthermore, an optically thick $e^-e^+\gamma$ plasma represents the Abelian analog of the non-Abelian quark-gluon plasma [8] currently investigated at large-scale accelerators.

The scenario for droplet creation can be visualized in the following way: Suppose that the radiation pressure of counter-propagating ultra-intense laser beams on a thin foil is so high that a substantial compression accompanied by sizeable pair creation is achieved. Estimates for such a process have been presented in [9]. Extrapolating these estimates one may envisage the idealized scenario of a hot and optically thick $e^-e^+\gamma$ plasma, with temperatures exceeding the 1 MeV scale. Optically thick $e^-e^+\gamma$ plasmas play an important role in the gamma ray bursts phenomena [10].

In [3] it has been pointed out that an $e^-e^+\gamma$ plasma droplet at initial temperatures T much larger than the electron mass m emits an intense gamma ray burst. However, the expansion dynamics was considered in [3] in a schematic manner. Nevertheless, the time structure and the spectrum of the burst depend crucially on the expansion dynamics of the plasma droplet driven by the thermodynamic pressure gradients. It is necessary to consider a realistic expansion dynamics as well as the particle production rates in the relativistic framework for a proper understanding of $e^-e^+\gamma$ plasmas produced in the laboratory and astrophysical sites such as gravitational collapse. The aim of the present paper is to quantify the droplet expansion dynamics by means of the relativistic hydrodynamics. This provides a realistic evaluation of the time evolution of the temperature profile and velocity profile. The latter one is important for properly accounting for the blue/red shift effects of the emitted photons.

Another avenue towards the creation of e^-e^+ plasma droplets has been envisaged in [6]

as a result of the dynamical Schwinger process. Due to the short (sub cycle) time scales the thermalization and the collective dynamics are not an issue. Instead, the emergence of e^-e^+ annihilation into γ pairs may be employed as diagnostic tool.

Our paper is organized as follows. In section II we consider the spherically symmetric expansion of plasma droplets within the relativistic hydrodynamics. This input is used in section III to estimate the spectrum of emitted photons. Section IV gives an account of the spectral emissivity for a warm plasma with a temperature in the order of the electron mass and focusses on the onset of the broadening of the 511 keV line when achieving higher temperatures. Section V is devoted to the summary. Appendix A presents the expansion dynamics with planar geometry.

II. RELATIVISTIC HYDRODYNAMICS

A sufficiently large $e^-e^+\gamma$ plasma droplet can be dealt with by means of relativistic hydrodynamics. The equations of motion imply local energy and momentum conservation expressed as

$$T^{\mu\nu}{}_{;\mu} = 0, \quad (1)$$

where $\mu, \nu = 0, \dots, 3$ denote Lorentz indices and a colon stands for the covariant derivative. For an isotropic medium (gas or fluid or plasma) the energy-momentum tensor reads

$$T^{\mu\nu} = (e + p)u^\mu u^\nu - pg^{\mu\nu} + \dots. \quad (2)$$

Here, the four-velocity is u^μ with normalization $u^\mu u_\mu = 1$ and $g^{\mu\nu}$ denotes the metric tensor, $\text{diag}(g^{\mu\nu}) = (1, -1, -1, -1)$ in Cartesian coordinates. The energy density is e , and p stands for the thermodynamic pressure. The ellipsis \dots in (2) denote dissipative terms being proportional to transport coefficients, such as shear and bulk viscosities, for instance. Neglecting the latter ones, (1, 2) can be solved once an equation of state is given. For $T > m$, the equation of state of a relativistic ideal gas can be employed, that is $e = 3p$. We consider a charge-symmetric plasma with zero net density. Accordingly, the chemical potential is zero, too. The pressure and temperature for our equation of state are related via $p = d_{eff} \frac{\pi^2}{90} T^4$ (we employ units with $\hbar = c = 1$) with $d_{eff} = 2 + \frac{7}{8}4$ for photons (first term) and electrons and positrons in equilibrium. This is the leading-order term in an expansion in powers of m/T .

Special symmetries simplify (1) tremendously. We consider here spherically symmetric droplets (planar slab geometry is considered in appendix A). Then (1) degenerates to two coupled equations, one for the pressure gradient and one for the radial velocity gradient. These equations can be solved by the methods of characteristics (cf. [11] for details). Numerical results are exhibited in Fig. 1.

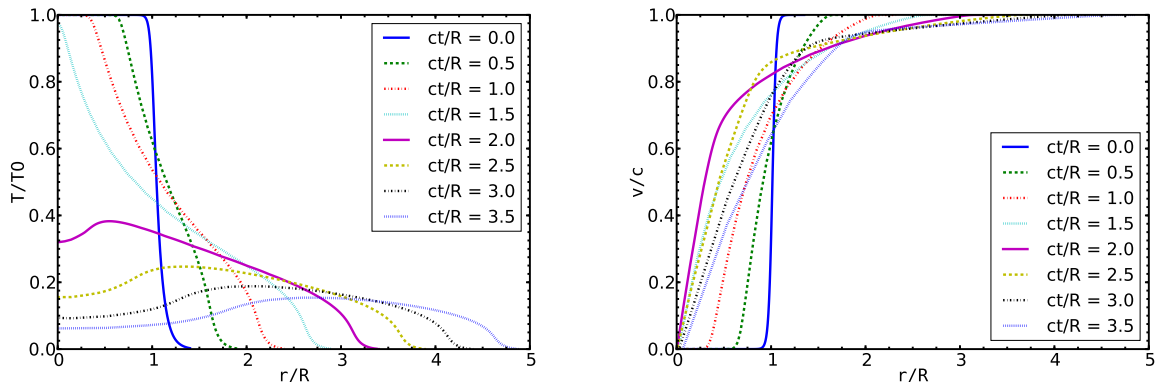


FIG. 1: Temperature (left) and velocity (right) profiles at various time instants for the spherically symmetric expansion.

The solution for the given equation of state can be represented for scaled quantities, T/T_0 and r/R , where T_0 and R stand for the initial temperature and radius, respectively, of the $e^-e^+\gamma$ droplet. We assume initially homogenous droplets, i.e. $T(t=0, r) = T_0$ for $r < R$ and $T(t=0, r) = 0$ for $r > R$. The initial radial profile is $v(t=0, r) = 0$ for $r < R$. Initially, a rarefaction wave travels towards the center with the velocity of sound $v_s = c/\sqrt{3}$ (corresponding to a Riemann type solution) and becomes reflected then, causing the non-trivial radial temperature profile with somewhat lower temperature in the center. We allow the temperature evolution until $\langle T \rangle \sim 0.1T_0$. For late times, the temperature drops further, but our assumed equation of state as well the photon rate below based on the perturbative estimates do not longer apply. These late times until disassembly are not important for the hard photon emission off the expanding droplet. The scaled time to cool from T_0 to $\langle T \rangle \sim 0.1T_0$ is about $ct = 3.5R$. That means, for instance, a droplet of initial radius $R = 2$ nm and $T_0 = 10$ MeV with energy content 13 kJ expands within the relaxation time for pairs and photon chemical equilibration, 0.025 fs, and cools to $\langle T \rangle \sim 1$ MeV.

The radial velocity profiles in Fig. 1 expose the rapid expansion of the cool surface layers

nearly at velocity of light. In particular, due to the rapid expansion, the droplet cools faster than what was assumed in the schematic model in [3]. This is reflected in the photon emission considered in the next section.

III. PHOTON EMISSION

Having at our disposal the realistic temperature and velocity profiles, we can now proceed to calculate the photon emission. It should be emphasized that the leakage of energy via photon emission is not properly accounted for in (1, 2) (cf. [12] for hydrodynamic schemes with energy leakage). It turns out however that the emitted energy during the considered evolution is small in comparison with the internal and kinetic energies so that a consistent hydrodynamic treatment with radiation transport analog to stellar core collapse simulations is not needed.

We employ the emission rate from thermo-field theory [13] (cf. figure 1 in [3])

$$\begin{aligned} \omega \frac{dN}{d^4x d^3k} = & \frac{2\alpha m_\infty^2 f_{+1}(\omega)}{(2\pi)^3} \left[\ln\left(\frac{T}{m_\infty}\right) + \frac{1}{2} \ln\left(\frac{2\omega}{T}\right) \right. \\ & \left. + C_{22} \left(\frac{\omega}{T}\right) + C_b \left(\frac{\omega}{T}\right) + C_a \left(\frac{\omega}{T}\right) \right], \end{aligned} \quad (3)$$

where $f_{+1}(\omega) = (\exp(\omega/T) + 1)^{-1}$ denotes the Fermi distribution function, and the dynamically generated asymptotic mass of the electron is $m_\infty^2 = 2m_{\text{th}}^2$. The thermal mass squared is determined by $m_{\text{th}}^2 = e^2 T^2 / 8$ with $e^2 = 4\pi\alpha$ and the C coefficients are given explicitly in [3]. $\hat{E}_\gamma = u^\mu k^\nu g_{\mu\nu}$ takes properly into account the red/blue shifts via the scalar product of the medium's four-velocity $u^\mu(t, \vec{x})$ and the photon's four-momentum $k^\nu = (\omega, \vec{k})$. The rate includes $2 \leftrightarrow 2$ Compton and annihilation processes (first three terms), bremsstrahlung processes (C_b) and off-shell pair annihilations processes (C_a).

The space-time integrated emission spectrum includes only such photons with a mean free path λ_γ being larger than the distance to the cool droplet surface in a given direction. The mean free path is locally determined by $\lambda_\gamma = \Gamma_\gamma^{-1}$ with the damping rate $\Gamma_\gamma(\omega) = \frac{(2\pi)^3}{4} e^{\omega/T} \frac{dN}{d^4x d^3k}$ which depends in turn on the photon energy.

The resulting energy-weighted photon spectrum is exhibited in Fig. 2. Similar to the schematic model [3] it extends beyond 50 MeV with notable strength. In contrast to [3], however, the maximum of the spectrum is an order of magnitude smaller. The origin of this difference may be traced back to the improved description of the droplet dynamics which

makes the droplet cooling considerably faster. The hard tail of the photon spectrum is emitted at early times and does not change at later times. In contrast, the softer part with $\omega \sim 10$ MeV gets significant contributions at later times. Comparing the spectra at $t = 4$ nm/c and $t = 7$ nm/c, one concludes that the very late radiation contribution for $T < 1$ MeV will contribute to photon energies $\omega < 5$ MeV.

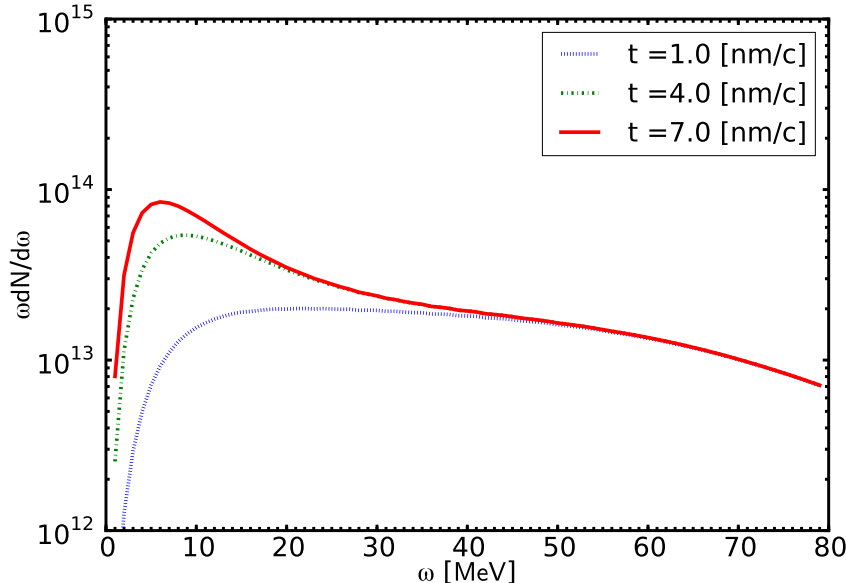


FIG. 2: Energy-weighted spectrum of emitted photons as a function of the energy for various times for $T > 1$ MeV.

IV. BROADENING OF THE 511 KEV LINE

The photon emission rate (3) applies for $T > m$, i.e. a hot plasma. In a warm plasma with $T \sim m$ or $T < m$, one expects a significant contribution from the annihilation process $e^-e^+ \rightarrow \gamma\gamma$. The corresponding inclusive photon rate for this process is obtained by the kinetic theory estimate

$$\begin{aligned} \omega \frac{dR}{d^4x d^3k} &= \frac{\mathcal{N}}{(2\pi)^7 16\omega} \int_{4m^2}^{\infty} \frac{ds}{s} \int_{t_{min}}^{t_{max}} dt |\mathcal{M}(s, t)|^2 \int_{\nu_{min}}^{\infty} d\nu (1 + f_{-1}(\nu - \omega)) \\ &\times \int_{E_{min}}^{E_{max}} dE \frac{f_{+1}(E) f_{+1}(\nu - E)}{\sqrt{(E_{max} - E)(E - E_{min})}} \end{aligned} \quad (4)$$

with $\mathcal{N} = 4$ and

$$t_{\min}^{\max} = m^2 - \frac{1}{2}s \left(1 \pm \sqrt{1 - \frac{4m^2}{s}} \right), \quad (5)$$

$$\nu_{\min} = \omega + \frac{s}{4\omega}, \quad t' = t - m^2, \quad (6)$$

$$E_{\min}^{\max} = \frac{-B \pm \sqrt{B^2 - 4AC}}{2A}, \quad (7)$$

$$A = -s^2, \quad B = 2s(\omega s + 2\omega t' - \nu t'), \quad (8)$$

$$C = st'(s + t') - \omega^2 s(s - 4m^2) - 2\omega \nu st' - \nu^2 t'^2 - 4\omega \nu m^2 s + s^2 m^2 \quad (9)$$

along with the additional kinematical restriction $-4s^2 t'(s + t')(1 + sm^2/((s + t')t')) > 0$. $\mathcal{M}(s, t)$ is the lowest-order invariant matrix element for the process $e^-e^+ \rightarrow \gamma\gamma$ (cf. [4]),

$$|\mathcal{M}(s, t)|^2 = 32\pi^2 \alpha^2 \left(\frac{m^2 - u}{m^2 - s} + \frac{m^2 - t}{m^2 - u} + 4\frac{m^2}{m^2 - t} + 4\frac{m^2}{m^2 - t} - 4 \left[\frac{m^2}{m^2 - t} + \frac{m^2}{m^2 - u} \right]^2 \right) \quad (10)$$

with $u = 2m^2 - s - t$, and the distribution functions are $f_{\mathcal{S}}(y) = (\exp\{y/T\} + \mathcal{S})^{-1}$. For $T \gg m$, corresponding to $m \rightarrow 0$, one recovers the form presented in [14]; the rate scales $\propto T^2$. In the opposite region $\omega \gg T$, where the Boltzmann approximation for the f_{+1} terms is justified [14], one finds

$$\begin{aligned} \omega \frac{dR}{d^4x d^3k} &= \frac{\mathcal{N}}{2(2\pi)^5} \frac{T}{\omega} e^{-\omega/T} \\ &\times \int_{4m^2}^{\infty} \frac{ds}{s} (s - 4m^2)^2 \sigma(s) \ln(1 - e^{-s/(4\omega T)})^{-1}, \end{aligned} \quad (11)$$

where the total cross section $\sigma(s)$ follows from integrating $d\sigma/dt = |\mathcal{M}|^2/(16\pi(s - 4m^2)^2)$ within $t_{\min} - t_{\max}$. Due to the interplay of the factors $e^{-\omega/T}$ and $\ln(1 - e^{-s/(4\omega T)})^{-1}$ in (11) the rate has a sharp maximum at $\omega = m$ for $T \ll m$. This is the 511 keV annihilation line, at very low temperatures, which broadens rapidly with increasing temperature. The high-frequency tail, $\omega \gg \max(T, m)$, behaves as $\omega dR/d^3k \propto e^{-\omega/T}$. The full width at half maximum is $\Delta\omega = \sqrt{-4mT \ln \frac{1}{2}}$, for $T \ll m$, with maximum $\propto e^{-2m/T}$.

The rate (4) is displayed in Fig. 3 for a sequence of temperatures. With increasing temperature the relative kinetic energy of the annihilating electron-positron pairs increases and, consequently, the photon energy increases in the medium's rest frame and becomes larger than m . This broadening of the 511 keV annihilation line, once isolated from other

processes with continuum radiation such as the Compton and the various bremsstrahlungs, may serve as a measure of the achieved temperature in a warm $e^-e^+\gamma$ plasma. At $T > 0.1m$, the broadened annihilation line changes gradually into a smooth continuum with typical exponential tail. For $T > m$, the maximum of the emission rate is shifted to $\omega > m$. The annihilation is then part of the complete rate (3).

The presented annihilation rates apply also to the transiently created e^-e^+ pairs by the dynamical Schwinger process, as envisaged in [6], when approximating the distribution functions by thermal ones.

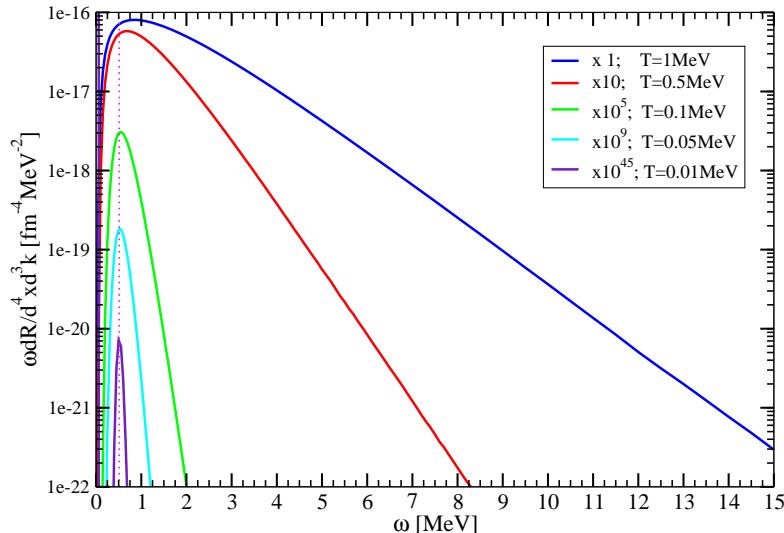


FIG. 3: Photon emission rate from e^-e^+ pair annihilation as a function of photon energy for various values of the temperature. Note the scale factors in the legend. The vertical dashed line indicates the position of 511 keV line.

V. SUMMARY AND DISCUSSION

In summary we consider the expansion dynamics of hot plasma droplets which can be created with next-generation ultra-intense laser beams. We present here the dynamics of charge-symmetric and equilibrium $e^-e^+\gamma$ plasma droplets by means of relativistic hydrodynamics. Our results support the estimate in [3] pointing to gamma flashes emitted off the

rapidly exploding droplets.

Clearly, our considered scenario is still idealized. The surplus of electrons over positrons needs to be considered in future analysis. This can be accommodated by a finite chemical potential steering the asymmetry of electrons and positrons. Furthermore, at given temperature, implying kinetic equilibrium, the positrons may not be chemically equilibrated. This requires an additional dynamical variable, e.g. a positron fugacity supplemented by appropriate rate equations. Also, ion impurities may have an impact on the plasma dynamics.

As indicated by the largely differing expansion time scales for spherical and plane expansion patterns, the flow symmetry may play an important role. To clarify that issue, more simulations are needed along with realistic initial conditions. The lessons learnt from the investigation of the quark-gluon plasma [8], however, indicate that it is useful to develop parallel with experiments the theoretical description after first initializing considerations.

Finally, we mention the broadening of the 511 keV line as useful tool for thermometry of small electron-positron-photon droplets produced in the laboratory and in astrophysical sites.

Acknowledgments

The authors thank T.E. Cowan and R. Sauerbrey for inspiring discussions. MGM is thankful to FZ Dresden-Rossendorf for support during the course of this work.

-
- [1] G.A. Mourou, T. Tajima, S.V. Bulanov, *Rev. Mod. Phys.* **78**, 309 (2006); Y.I. Salamin, S.X. Hu, K.Z. Hatsagortsyan, C.H. Keitel, *Phys. Rep.* **427**, 41 (2006); M. Marklund, P.K. Shukla, *Rev. Mod. Phys.* **78**, 309 (2006); G. Gregori et al., *High Energy Density Phys.* **6**, 166 (2010).
 - [2] I. Kuznetsova, D. Habs, J. Rafelski, *Phys. Rev. D* **78**, 014027 (2008).
 - [3] M.G. Mustafa, B. Kämpfer, *Phys. Rev. A* **79**, 020103(R) (2009).
 - [4] I. Kuznetsova, D. Habs, J. Rafelski, *Phys. Rev. D* **81**, 053007 (2010).
 - [5] A.G. Aksenov, R. Ruffini, G.V. Vereshchagin, *Phys. Rev. E* **81**, 046401 (2010).
 - [6] D.B. Blaschke, G. Röpke, S.M. Schmidt, S.A. Smolansky, A.V. Tarakanov, arXiv:1006.1098 [physics.plasma-ph];

- D.B. Blaschke et al., Eur. Phys. J. D 55, 341 (2009).
- [7] M.H. Thoma, Rev. Mod. Phys. 81, 959 (2009).
- [8] Quark Matter 2009 - The 21st International Conference on Ultrarelativistic Nucleus-Nucleus Collisions, Nucl. Phys. A 830, 1c (2009),(Eds.) P. Stankus et al.
- [9] B. Shen, J. Meyer-ter-Vehn, Phys. Rev. E 65, 016405 (2001).
- [10] R. Ruffini, G. Vereshchagin, S.-S. Xue, Phys. Rep. 487, 1 (2010).
- [11] G. Baym, B.L. Friman, J.P. Blaizot, M. Soyer, Nucl. Phys. A 407, 541 (1983), J.P. Blaizot, J.Y. Ollitrault, Nucl. Phys. A 458, 745 (1986).
- [12] H.W. Barz, B. Kämpfer, L.P. Csernai, B. Lukacs, Nucl. Phys. A 465, 742 (1987); B. Kämpfer, H.W. Barz, B. Lukacs, Exp. Tech. Phys. 35, 13 (1987).
- [13] P. Arnold, G.D. Moore and L.G. Yaffe, J. High. Energy Phys. 12, 009 (2001).
- [14] J. Kapusta, P. Lichard, D. Seibert, Phys. Rev. D 44, 2774 (1991).

Appendix A: Planar Slab Geometry

A one-dimensional planar expansion (cf. [11]) needs a much longer time to cool the system down to T_0 to $\langle T \rangle \sim 0.1T_0$. This is exhibited in Figs. 4 and 5.

To understand qualitatively this huge difference to the spherically symmetric expansion, one may mention that for the latter one an increase of the radius by a factor of $10^{4/3}$ is needed to cool the medium from T_0 to $0.1T_0$ when neglecting the conversion of internal energy into kinetic energy and emission. For planar geometry, in contrast, the thickness of a slab must increase by a factor 10^4 . This estimates explain the much longer time scales to cool the medium to a tenth of the initial temperature. Of course, the transverse expansion of a finite slab of matter will become important and requires more involved multi-parameter solutions of the hydrodynamical expansion.

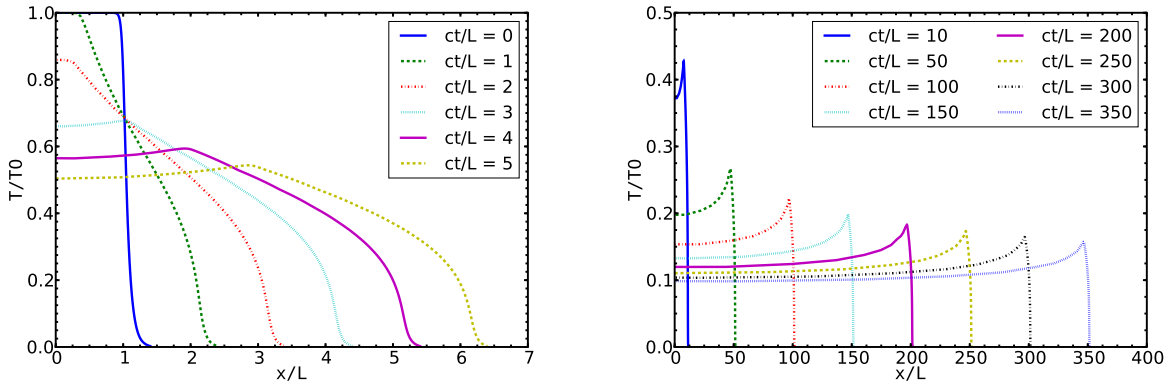


FIG. 4: Temperature profiles at various time instants for a planar one-dimensional expansion. Left (right): short (long) times.

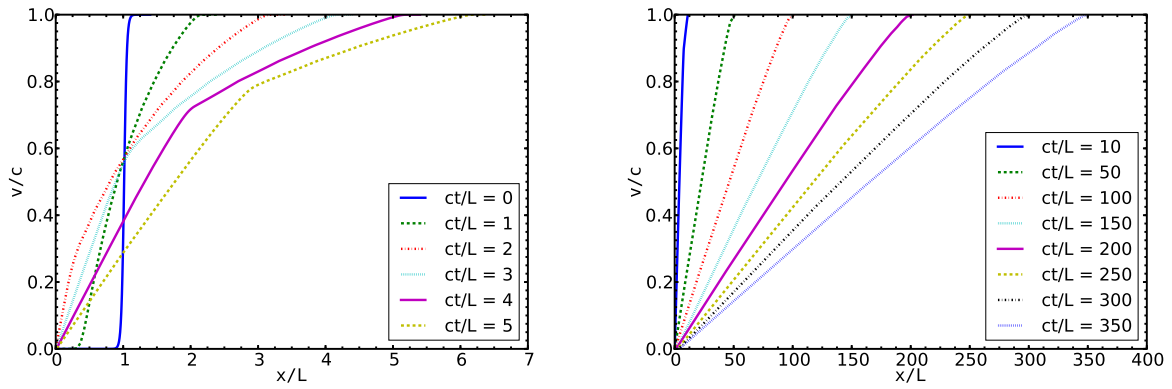


FIG. 5: Velocity profiles at various time instants for a planar one-dimensional expansion. Left (right): short (long) times.